Check for updates

Glutaraldehyde cross-linked CDA/HBP-NH$_2$ nanofiber membrane for adsorption of heavy metal ions in wastewater

Zang Chuanfeng,†[a] Han Xiangye,†[a] Dong Erying,[b] Shen Feiyu,[a] Yan Tingting,*[a] Wang Runyue[a] and Zhang GuangyuYu [ID] *[a]

A new type of nanofiber membrane was prepared by mixed electrospinning of cellulose diacetate and amino-terminated hyperbranched polymer (HBP-NH$_2$), and glutaraldehyde (GA) crosslinking was used to improve its water resistance and shape retention. pH, adsorption time, and initial solution concentration on Cu(II) and Cr(VI) ions were studied. Results showed that the prepared GA-CDA/HBP-NH$_2$ nanofiber had good spinning uniformity, hydrophilicity, and adsorption effect on Cu(II) and Cr(VI) ions compared with the pure CDA nanofiber. The maximum adsorption capacity of GA-CDA/HBP-NH$_2$ for Cu(II) and Cr(VI) was 50.2 and 176.6 mg g^{-1}, respectively.

1. Introduction

With the rapid development of industry, considerable wastewater is discharged, resulting in a sharp increase in the content of heavy metal ions such as Cu(II) and Cr(VI) in natural water sources. The heavy metal ions in wastewater are toxic and difficult to remove, and they exist in water for a long time, which is harmful to the environment and human life and health. Even at a trace level in water, these heavy metal ions will have a serious impact on biological health. They may also cause damage to tissues and organs and endanger lives.[1–3] At present, the main methods to remove heavy metal ions from waste are chemical precipitation, electrochemical reduction, ion exchange, membrane separation, and adsorption.[4–7] Among the methods, the chemical precipitation method requires the addition of a large amount of chemicals, and the sludge produced by the precipitation will increase the processing cost; electrochemical reduction has high cost and low efficiency; ion exchange has high cost, limited scope of application, and high requirements for sewage. In addition, membrane separation primarily includes electrodialysis and reverse osmosis. Although electrodialysis has high filtration efficiency and the membrane of electrodialysis can be recycled, the amount of water treated is small and the cost is high. The reverse osmosis method has high removal rate and simple operation, but the membrane has low strength, short life, and is easy to be blocked. The adsorption method is considered to be an effective

means to remove heavy metals due to its simple preparation, low cost, high selectivity, and reusable adsorbents.[8–11]

At present, the combination of nanofiber adsorbent and electrospinning technology has great potential in wastewater treatment.[12,13] Electrospinning has the characteristics of simple operation, high efficiency, low cost, and strong versatility. It is a commonly used method for preparing nanofiber membranes.[14,15] In addition, the spinning membrane has large specific surface area, high porosity, good permeability, adjustable pore structure, and easy surface functionalization.[16,17] Moreover, the composition and structure of electrospun nanofiber films can be modified to obtain satisfactory adsorption properties.[18–20]

Cellulose is a natural polymer substance with high crystallinity and insolubility in water. It is non-toxic, and it can appear in the form of powder, flake, membrane, and fiber; thus, cellulose is widely used as a matrix material.[21] As a cellulose derivative, cellulose diacetate (CDA) is non-toxic and harmless; thus, it is often used as filtering equipment such as glasses frame, handle, packaging film, cigarette filter tip, microporous filter membrane, and electrospinning material.

Hyperbranched polymers (HBP) are highly branched three-dimensional macromolecular materials. Compared with linear and crosslinked analogs, HBP have more branching points; molecular chains cannot be easily entangled; viscosity does not change with the increase of molecular weight, and HBP was rich in terminal functional groups.[22] Hyperbranched polymers have been widely used in the fields of coatings, nanotechnology, additives, and biomaterials.[23] Given their rich functional groups and good chelating properties, HBP have been considered as an effective way to design and prepare new heavy metal ion adsorbents in recent years. Moreover, HBP can improve the synthesis of a variety of functional materials.[24,25] Amino-

terminated hyperbranched polymers (HBP-NH$_2$) have rich amino functional groups, which can chelate with a variety of heavy metals to remove heavy metal ions from water.

Zang[26] et al. used spun CDA nanofibers as raw materials. After argon plasma treatment, a large number of active free radicals were formed on the surface of CDA nanofibers. Using glutaraldehyde (GA) crosslinking, HBP, which are rich in amino groups, were grafted onto CDA nanofibers to prepare HBP-NH$_2$-modified CDA nanofiber adsorption materials. The adsorption capacity of Cu(II) ion in cationic form and Cr(VI) ion in water primarily in the form of Cr$_2$O$_7^{2-}$, CrO$_4^{2-}$, and HCrO^{4-} was investigated. Tian[27] et al. crosslinked PVA electrospun nanofiber membrane with GA solution. The effects of crosslinking time and concentration of metal ion solution on the adsorption of Cu(II) and Cr(VI) were studied.

In this paper, a new type of nanofiber membrane was prepared by mixed electrospinning of CDA and amino-terminated hyperbranched polymer (HBP-NH$_2$). Glutaraldehyde-crosslinked CDA/HBP-NH$_2$ nanofiber membrane (GA-CDA/HBP-NH$_2$) was prepared by GA vacuum crosslinking to improve its water resistance and shape retention. The formation of GA-CDA/HBP-NH$_2$ and the adsorption effects of different adsorbents, pH, adsorption time, and initial solution concentration on Cu(II) and Cr(VI) ions were investigated.

2. Experimental

2.1. Materials

N,N-Dimethylacetamide(DMAc, AR = 99.0%) and trifluoroacetic acid were purchased from Aladdin Reagent (Shanghai) Co., Ltd. Acetone (CP) was purchased from Shanghai Lingfeng Chemical Reagent Co., Ltd. Cellulose diacetate (CDA) was purchased from Nantong Acetate Fiber Co., Ltd. Hyperbranched polymer (HBP-NH$_2$) was prepared by ourselves. GA (25%) and copper nitrate (Cu(NO$_3$)$_2$·3H$_2$O) were purchased from Sinopharmaceutical Group Chemical Reagent Co., Ltd. Potassium dichromate (K$_2$Cr$_2$O$_7$, GR) was purchased from Tianjin Zhiyuan Chemical Reagent Co., Ltd.

2.2. Preparation of CDA/HBP-NH$_2$ electrospun nanofiber membrane

CDA was dissolved in the mixed solution of CP and DMAc (2 : 1) to form a spinning solution of 8%, and then the HBP was dissolved in a certain proportion in the spinning solution. The prepared solution was transferred to a 10 mL syringe using a no. 25 needle, and the voltage was 18 kV. The distance between the needle and the receiving plate was 20 cm, and the speed of the microinjection pump was 0.015 mL min^{-1}. The electrospinning film was removed from the receiving plate and baked in a vacuum drying box at 60 °C for 2 h to remove the residual solvent and sealed for later use.

2.3. Preparation of glutaraldehyde-crosslinked CDA/HBP-NH$_2$ nanofiber membrane (GA-CDA/HBP-NH$_2$)

The nanofiber membrane was separated from the surface of aluminum foil, and then the nanofiber membrane was placed in a vacuum drying dish with 25% GA solution at the bottom of the drying dish, in which trifluoroacetic acid was dripped, and the vacuum was extracted and placed for 72 h. Finally, the crosslinked nanofiber membrane was removed, washed, and dried with deionized water to prepare the GA-crosslinked CDA/HBP-NH$_2$ nanofiber membrane (GA-CDA/HBP-NH$_2$).

2.4. Characterization and adsorption experiments

A field-emission scanning electron microscope (Gemini SEM300, Germany) was used to observe the surface micro-morphology and surface element analysis (EDS), and gold was sprayed on the samples before observation. Fourier transform infrared (FT-IR) spectrum was measured in the 400–4000 cm^{-1} range using a Fourier transform infrared spectrometer (Nicolet, Thermo Scientific, Madison, WI, USA). An X-ray photoelectron spectrometer (XPS, Kratos Axis Ultra DLD, UK) was used to analyze the surface chemical composition of the sample. The contact angle was measured using a contact angle measuring instrument (Dataphysics OCA15EC, Germany).

A certain amount of copper nitrate (Cu(NO$_3$)$_2$·3H$_2$O) and potassium dichromate (K$_2$Cr$_2$O$_7$) was dissolved in deionized water to prepare Cu(II) and Cr(VI) solutions of 100 ppm. The remaining concentrations of Cu(II) and Cr(VI) solutions needed in the experiment can be obtained by diluting the prepared 100 ppm solution. The adsorption experiments were conducted on the water bath shaker, and the shaking speed of the water bath shaker was 100 rpm. The experimental conditions were adjusted to test the effects of different adsorbents, pH, contact time, and initial liquid concentration on adsorption. The concentration of heavy metal ion solution was measured using an atomic absorption spectrophotometer (Shimadzu, AA-6880, Japan). The concentration of heavy metal ions was determined as follows:

$$q_t = \frac{(C_0 - C_t) \times V}{m}$$

$$q_e = \frac{(C_0 - C_e) \times V}{m}$$

where q_t (mg g^{-1}) and q_e (mg g^{-1}) are the adsorption capacity of heavy metal ions at any time t and equilibrium. C_0 (mg L^{-1}) is the initial solution concentration; C_t (mg L^{-1}) refers to the concentration at time t; C_e (mg L^{-1}) represents equilibrium concentrations. V (mL) is the volume of heavy metal solution, and m (g) is the adsorbent mass.

In testing the effect of adsorbent on the adsorption of heavy metal solution under different pH, 0.01 g of GA-CDA/HBP-NH$_2$ was added to a conical bottle of copper nitrate (30 ppm) or potassium dichromate (30 ppm) containing 50 mL, and the pH of the adsorption solution was adjusted to 2.0, 2.5, 3, 3.5, 4, 4.5, 5, 5.5, 6, and 6.5 with 0.1 M HCl and 0.1 M NaOH. The supernatant was diluted after adsorption under constant temperature oscillation for 6 h. The residual amount of metal ion solution was measured.

For the contact time, 0.05 g of the GA-CDA/HBP-NH$_2$ nanofiber membrane was added to the conical bottle. Copper nitrate

(30, 60, and 100 ppm) and potassium dichromate (30, 60, and 100 ppm) solutions were added to 50 mL, and their initial pH was 5.5 and 4.0, respectively. Ten parallel experiments were conducted at different contact time (30, 60, 90, 120, 150, 180, 240, 300, 360, and 480 min).

At different initial concentrations (10, 20, 30, 60, and 100 ppm), 0.01 g of GA-CDA/HBP-NH$_2$ was added into a 50 mL solution containing Cu(II) (pH 5.5) and Cr(VI) (pH 4.0). Five parallel experiments were conducted under the contact time of 8 h.

3. Results and discussion

3.1. Characterization of the CDA/HBP-NH$_2$ nanofibers

Given the large amount of amino functional groups, HBP-NH$_2$ can be easily dissolved in water. The CDA/HBP-NH$_2$ nanofiber prepared by electrospinning exhibited poor water resistance. Thus, the nanofiber membrane was crosslinked with GA to address the defect. Fig. 1 shows the configuration and spinning of GA-CDA/HBP-NH$_2$ solution and the whole adsorption process after crosslinking. During the mixed spinning of CDA and HBP-NH$_2$, HBP-NH$_2$ crosslinked to the fiber surface by GA, whereas the surface of HBP-NH$_2$ was rich in amino groups, which will produce electrostatic adsorption with Cu(II) and Cr(VI) in wastewater, thereby providing high adsorption for heavy metal ions.

The nanostructure and morphology of nanofibers prepared with different proportions of CDA and HBP-NH$_2$ were first examined under FESEM, and the result is shown in Fig. 2. As shown in Fig. 2(a), the diameter of pure CDA fiber is small, and many beads are found in the fiber netting. These beads are formed by the unevenness of fiber drawing in electrospinning. Fig. 2(b–e) shows that when CDA is added to HBP-NH$_2$, the diameter of the fiber increases, and the beads disappear. Moreover, spinnability is improved at the same CDA concentration, and traces of HBP-NH$_2$ appear on the fiber surface. When the fiber is electrospun, HBP-NH$_2$ will transfer to the surface, and with the increase of HBP-NH$_2$ concentration, the fiber diameter gradually increases. However, with the increase of HBP-NH$_2$ concentration, the fiber morphology changes. The adhesion among the fibers increases, and the surface area of the nanofiber membrane decreases. Therefore, we select
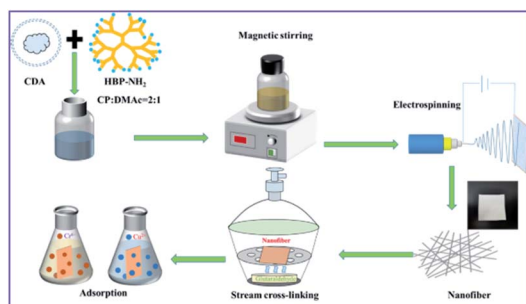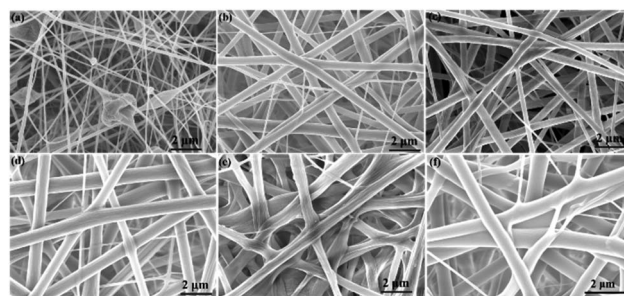

Fig. 2 SEM images of CDA/HBP-NH$_2$ with different proportions (a) 1 : 0, (b) 1 : 1.5, (c) 1 : 2, (d) 1 : 2.5, (e) 1 : 3 and (f) 1 : 2.5 cross-linked with GA.

CDA : HBP-NH$_2$ = 1 : 2.5 as the crosslinking object. Fig. 2(f) shows the SEM image of CDA/HBP-NH$_2$ nanofiber membrane with ratio of 1 : 2.5 after cross-linked with glutaraldehyde. Compared with CDA/HBP-NH$_2$ shown in Fig. 2(d), the surface of the GA-CDA/HBP-NH$_2$ nanofiber is smooth, and the fiber diameter is larger.

The functional groups on the electrospun membrane were characterized by FT-IR. As shown in Fig. 3, compared with the CDA film, a new peak at 1673 cm^{-1} belonging to C=N appeared in the GA-CDA/HBP-NH$_2$ nanofiber membranes. In addition, a wide absorption peak was observed between 3100 and 3500 cm^{-1}, which is the stretching vibration absorption peak of N–H formed by the overlap of free-NH$_2$ and –NH and associated-NH$_2$ and NH. The hydrogen bond formed by associating amine weakens the strength of N–H and shifts the absorption peak of N–H stretching vibration to a low wavenumber band.[28] The bending vibration absorption peak of N–H appeared at the absorption frequency of 1559 cm^{-1} for GA-CDA/HBP-NH$_2$, indicating the presence of primary amine in the modified CDA. These results indicated that GA successfully crosslinked CDA/HBP-NH$_2$ nanofibers.

Fig. 4 shows the EDS diagrams of different adsorbents. From Fig. 4(a), we can see that the surface of pure CDA only contains carbon (C) and oxygen (O) elements. The GA-CDA/HBP-NH$_2$ in
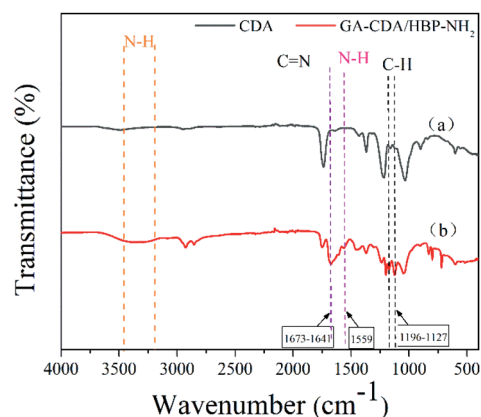

Fig. 1 Schematic diagram of the preparation and crosslinking of electrospun membranes and the adsorption of heavy metal ions.

Fig. 3 FT-IR diagrams of (a) CDA and (b) GA-CDA/HBP-NH$_2$ nanofibers.

Fig. 4(b) contains carbon (C) and oxygen (O) as well as nitrogen (N), indicating that it is the result of glutaraldehyde cross-linking HBP-NH$_2$.

X-ray photoelectron spectroscopic analyses of the CDA and GA-CDA/HBP-NH$_2$ nanofiber were conducted to investigate GA crosslinking. Fig. 5 shows the X-ray photoelectron spectroscopy of CDA and GA-CDA/HBP-NH$_2$ nanofiber films and further compares the elemental composition of the modified nanofiber films. As shown in Fig. 5(a), CDA nanofiber films show C 1s and O 1s photoelectron lines at 286.2 and 532.6 eV, respectively, because CDA nanofiber films contain only C and O, whereas GA-CDA/HBP-NH$_2$ nanofiber membranes show evident N 1s photoelectron lines at 398.6 eV, indicating the successful preparation of GA-crosslinked CDA/HBP-NH$_2$. Fig. 5(b) shows the peaks of C 1s in CDA nanofibers. It can be seen from the figure that CDA has chemical bonds corresponding to C–C, C–O and C=O at 284.8 eV, 286.4 eV and 288.7 eV, respectively. Fig. 5(c) shows the peaks of C 1s in GA-CDA/HBP-NH$_2$ nanofibers. GA-CDA/HBP-NH$_2$ has chemical bonds corresponding to C–C and C–N at 284.3 eV and 285.5 eV. The appearance of C–N bonds in GA-CDA/HBP-NH$_2$ nanofibers further confirmed the successful preparation of glutaraldehyde cross-linked CDA/HBP-NH$_2$.

Fig. 6 shows the contact angles of different adsorbents. The contact angle of the adsorbent shows its affinity for heavy metal ion solution adsorption. Materials with high hydrophilicity can make the heavy metal ion solution easier to enter the inside of the fiber membrane. The contact angle of CDA nanofiber membrane is 147.9°, showing super hydrophobicity. The contact angle of CDA/HBP-NH$_2$ is only 15.3°, because the fiber surface contains a lot of amino groups, so it is hydrophilic. The contact angle of GA-CDA/HBP-NH$_2$ is 67.6°. This may be because the cross-linking of glutaraldehyde will cause part of the amino groups on the surface of the nanofibers to be reacted.
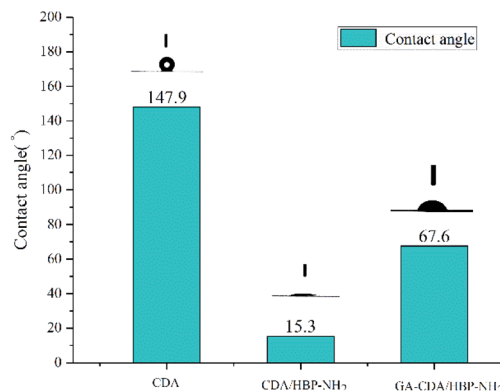

Fig. 6 Contact angle of CDA, CDA/HBP-NH$_2$ and GA-CDA/HBP-NH$_2$ nanofibers.

The decrease in the amount of amino groups reduces the hydrophilicity, so the contact angle get bigger. However, compared with the CDA fiber membrane, the crosslinked nanofiber membrane has increased hydrophilicity, which is beneficial to the adsorption of heavy metal ions.

3.2. Adsorption performance and the effect of pH, adsorption time, and initial liquid concentration on the adsorption performance of GA-CDA/HBP-NH$_2$

3.2.1 Adsorption performance test. The adsorption capacity of Cu(II) and Cr(VI) by CDA and GA-CDA/HBP-NH$_2$ nanofiber membranes was studied. As shown in Fig. 7, the adsorption capacity of Cu(II) and Cr(VI) on the nanofiber membrane spun with GA-CDA/HBP-NH$_2$ was greatly improved. The adsorption effect of Cu(II) on the CDA nanofiber membrane is almost zero. After the GA-CDA/HBP-NH$_2$ nanofiber membrane is crosslinked with GA, the structure of the nanofiber membrane is stable, and the adsorption efficiency is greatly improved; the maximum capacity can reach 50.2 mg g^{-1}. For Cr(VI), the maximum capacity can reach 176.6 mg g^{-1}, whereas the adsorption capacity of the GA-CDA/HBP-NH$_2$ nanofiber membrane is four times that of the CDA nanofiber. In addition, the unmodified CDA nanofiber membrane adsorbs Cr(VI) to a certain extent probably because the CDA nanofiber has high specific surface area and high surface energy.

3.2.2 Effects of pH on the adsorbent. The pH of the solution is an important factor affecting the adsorption capacity of the adsorbent, which affects not only the existing form of metal ions in the solution, but also the surface characteristics of the adsorbent.[29] Fig. 8(a) shows the effect of the initial pH on the adsorption capacity. GA-CDA/HBP-NH$_2$ is a weakly basic adsorbent because it is rich in weakly basic amino functional groups. For Cu(II), the adsorption capacity of the GA-CDA/HBP-NH$_2$ adsorbent increases initially and then decreases because the hydrated hydrogen ion (H$_3$O$^+$) in the solution binds closely to the amino functional group on the adsorbent when the pH is low. The binding of the amino functional group to the Cu(II) metal ion in the solution is limited by the charge repulsion force. With the increase of pH to 5.5, the amino functional
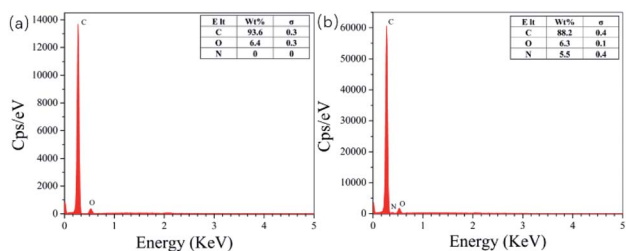

Fig. 4 EDS diagram of different adsorbents: (a) CDA and (b) GA-CDA/HBP-NH$_2$ nanofibers.

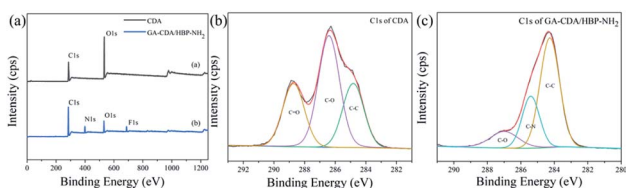**Fig. 5** (a) High-resolution XPS spectra and (b) C 1s of CDA and (c) C 1s of GA-CDA/HBP-NH$_2$.
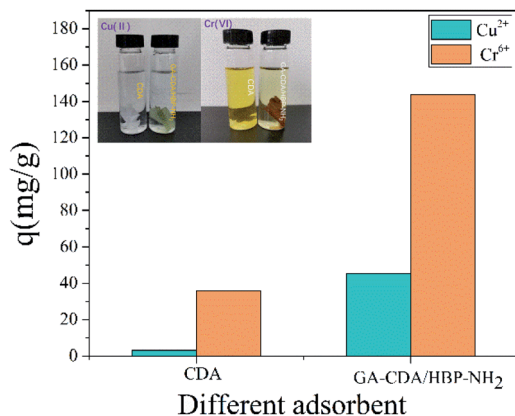
Fig. 7 Adsorption capacity of CDA and GA-CDA/HBP-NH$_2$ for Cu(II) and Cr(VI) ions.
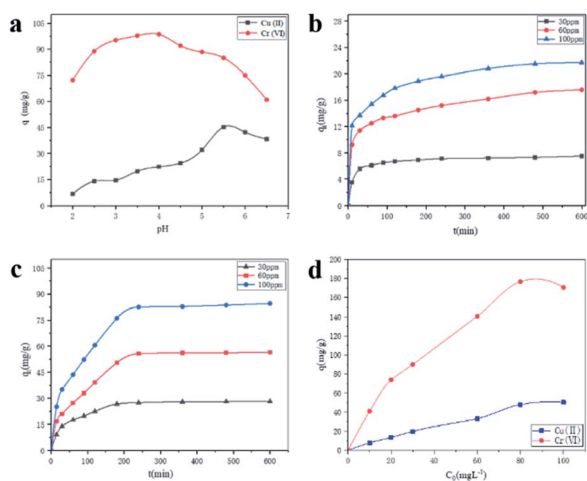

Fig. 8 Adsorption performance of the GA-CDA/HBP-NH$_2$ membrane at (a) different pH. (b) Adsorption of Cu(II) ions at different adsorption times. (c) Adsorption of Cr(VI) ions at different adsorption times and (d) initial solution concentrations.

groups on the adsorbents began to be deprotonated, resulting in more free amino functional groups binding to heavy metal Cu(II) ions through complexation. For Cr(VI), the adsorption capacity of the GA-CDA/HBP-NH$_2$ adsorbent increased initially and then decreased with the increase of pH value and reached the maximum at pH 4.0. When pH was low, the protonation degree of the amino functional groups on the GA-CDA/HBP-NH$_2$ adsorbent increased, and protonated NH$_3^+$ ions were formed, whereas Cr(VI) in solution primarily existed in the form of HCrO$_4^-$. Therefore, the two were combined by electrostatic attraction and complexation. Therefore, based on the test, all the experiments were conducted under the optimal pH after determining the optimal adsorption pH of each solution, that is, the initial pH was 5.5 (Cu(II)) and 4.0 (Cr(VI)).

3.2.3 Adsorption time. Adsorption time is an important index to measure the adsorption performance of adsorbents, and the adsorption time directly affects the adsorption capacity. As shown in Fig. 8(b), for Cu(II), a large number of active
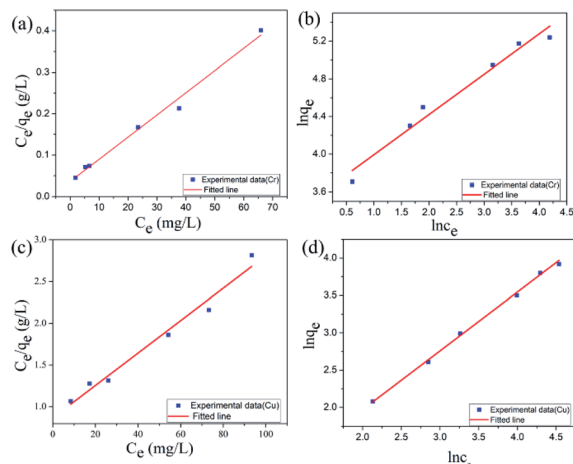

Fig. 9 Fitting line of the adsorption isotherm of the GA-CDA/HBP-NH$_2$ membrane for (a and b) Cu(II) ion solution and (c and d) Cr(VI) ion solution. (a and c) Langmuir adsorption isotherm fitting line. (b and d) Freundlich adsorption isotherm fitting line.

adsorption centers are found on the surface of the GA-CDA/HBP-NH$_2$ adsorbent at the beginning of adsorption, which adsorbs heavy metal ions rapidly in 30 min. The adsorption rate slows down after 30 min and tends to smooth after 480 min, but it still has an upward trend. As shown in Fig. 8(c), for Cr(VI), the adsorption rate increases rapidly in 180 min and finally reaches the adsorption equilibrium after 240 min. In addition, we increase the amount of adsorbent to 0.5 g to ensure enough adsorption active sites and verify the difference in adsorption capacity at different concentrations but at the same adsorption time. At different concentrations, the adsorption capacity of Cu(II) and Cr(VI) increases with the increase of concentration at the same adsorption time. However, the presence of many adsorbents affects the calculation of adsorption capacity; therefore, exploring the optimal adsorption concentration and the amount of adsorbent is necessary.

3.2.4 Effects of initial liquid concentration on the performance of adsorbents. The adsorption capacity of the solution will also be affected by the initial solution concentration; therefore, determining the optimum concentration of the adsorbent is important. As shown in Fig. 8(d), the adsorption capacity of the adsorbent increases gradually with the increase of the initial concentration. For Cu(II), when the solution concentration is 80 mg L^{-1}, the adsorption capacity is almost unchanged; therefore, the optimum adsorption concentration of Cu(II) is 80 mg L^{-1}. For Cr(VI), the solution also reaches the best adsorption concentration of 80 mg L^{-1}. Therefore, the best adsorption concentration of the adsorbent for Cu(II) and Cr(VI) solution is 80 mg L^{-1}.

3.2.5 Adsorption isotherm. The Langmuir model and Freundlich model were used to analyze the adsorption data obtained from the adsorption experiment and understand the interaction between adsorption sites and heavy metal ions.

The Langmuir adsorption isotherm model is shown in the following equation:

Table 1 Langmuir and Freundlich parameters of GA-CDA/HBP-NH$_2$ for Cu(II) and Cr(VI) adsorption

Metal ions	Langmuir model			Freundlich model		
	K_L (L mg^{-1})	q_m (mg g^{-1})	R^2	$1/n$	K_F	R^2
Cu(II)	0.00759	122.85	0.86486	0.78791	1.48372	0.99471
Cr(VI)	0.14923	186.22	0.99075	0.42821	35.33592	0.97244

$$\frac{c_e}{q_e} = \frac{c_e}{q_m} + \frac{1}{K_L q_m}$$

The Freundlich adsorption isotherm model is shown in the following equation:

$$\ln q_e = \frac{1}{n} \ln c_e + \ln K_F$$

where c_e is the equilibrium concentration of heavy metal ions (mg L^{-1}); q_e is the adsorption amount of heavy metals when the adsorption equilibrium of the adsorbent is reached (mg g^{-1}); K_L is the adsorption equilibrium constant of Langmuir (L mg^{-1}); K_F is the adsorption capacity coefficient of Freundlich, and $1/n$ is the characteristic constant related to the adsorption intensity.

The linear fitting curves of Langmuir and Freundlich isothermal adsorption of Cu(II) ions by GA-CDA/HBP-NH$_2$ adsorbents are shown in Fig. 9(a and b), and the linear fitting parameters are shown in Table 1. Based on the fitted linear correlation coefficient (R^2), the fitting curve of the adsorption isotherm of GA-CDA/HBP-NH$_2$ to heavy metal Cu(II) ions has a good correlation with the Freundlich equation, and the linear correlation coefficient (R^2) is 0.996, whereas the correlation between the adsorption isotherm and the Langmuir equation is poor. Moreover, the linear correlation coefficient (R^2) is only 0.86. As shown in Table 1, the value of $1/n$ is less than 1, indicating that the adsorption of Cu(II) ions by GA-CDA/HBP-NH$_2$ adsorbents is easy.

The linear fitting curves of Langmuir and Freundlich isothermal adsorption of Cr(II) ions by GA-CDA/HBP-NH$_2$ adsorbents are shown in Fig. 9(c and d), and the linear fitting parameters are shown in Table 1. Based on the fitted linear correlation coefficient (R^2), the fitting curve of the adsorption isotherm of GA-CDA/HBP-NH$_2$ to heavy metal Cr(II) ions has a good correlation with the Langmuir equation, and the linear correlation coefficient (R^2) is 0.99. The correlation between the adsorption isotherm and the Freundlich equation is also high, and the linear correlation coefficient (R^2) is 0.97. As shown in Table 1, the value of GA-CDA/HBP-NH$_2$ is between 0.1 and 0.5. Therefore, the adsorption of Cr(II) ions by the GA-CDA/HBP-NH$_2$ adsorbent is multi-layer, and the GA-CDA/HBP-NH$_2$ adsorbent has a good adsorption property to Cr(VI) ion.

3.2.6 Adsorption kinetics. The Lagergren quasi-first-order kinetic equation and quasi-second-order kinetic equation were used to fit the experimental data of GA-CDA/HBP-NH$_2$ for Cu(II) and Cr(VI) ions and to study the adsorption mechanism. According to the fitting correlation coefficient (R^2), the

significance of fitting was tested, and the adsorption performance of GA-CDA/HBP-NH$_2$ was evaluated (Fig. 10).

The Lagergren quasi-first-order kinetic equation was presented as follows:

$$\ln (q_e - q_t) = \ln q_e - K_1 t$$

Lagergren pseudo-second-order kinetic equation was given as follows:

$$\frac{t}{q_t} = \frac{1}{K_2 q_e^2} + \frac{t}{q_e}$$

where q_e is the amount of heavy metals adsorbed when the adsorbent reaches equilibrium (mg g^{-1}); q_t is the amount of heavy metals adsorbed by the adsorbent at time t (mg L^{-1}); K_1 is the quasi-first-order adsorption rate constant (min^{-1}); K_2 is the quasi-second-order adsorption rate constant (mg [g min]$^{-1}$).

The adsorption data of Cu(II) ions with different concentrations of adsorbents are fitted, and the relevant data are shown in Table 2. As shown in Table 2, R^2 obtained by quasi-second-order kinetic equation regression fitting is greater than 0.996, which is better than that obtained by quasi-first-order kinetic equation. In addition, the equilibrium adsorption capacity of Cu(II) ions obtained from heavy metal adsorption experiments
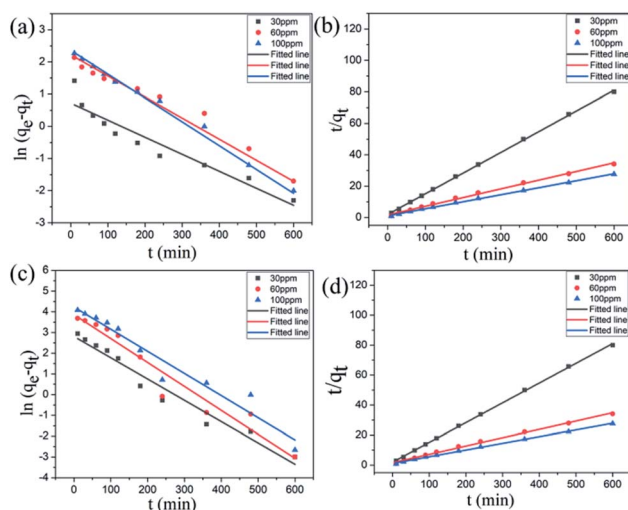

Fig. 10 Adsorption performance of the GA-CDA/HBP-NH$_2$ membrane at different concentrations: (a and b) Cu(II) ion solution, (c and d) Cr(VI) ion solution, (a and c) pseudo-first-order model, and (b and d) pseudo-second-order model.

Table 2 Kinetic parameters of GA-CDA/HBP-NH$_2$ adsorption of Cu(II) ions at different concentrations

Concentration	Pseudo-first-order model			Pseudo-second-order model		
	q_e (mg g^{-1})	K_1 (min^{-1})	R^2	q_e (mg g^{-1})	K_2 (min^{-1})	R^2
30 ppm	2.1	0.00529	0.9033	7.59	0.00888	0.99963
60 ppm	8.55	0.00592	0.97091	18.05	0.00189	0.996
100 ppm	10.23	0.00709	0.99293	22.40	0.00177	0.99837

Table 3 Kinetic parameters of GA-CDA/HBP-NH$_2$ adsorption of Cr(VI) ions at different concentrations

Concentration	Pseudo-first-order model			Pseudo-second-order model		
	q_e (mg g^{-1})	K_1 (min^{-1})	R^2	q_e (mg g^{-1})	K_2 (min^{-1})	R^2
30 ppm	16.57	0.01026	0.96007	30.3	0.001	0.99796
60 ppm	47.63	0.01155	0.94371	63.01	0.00028	0.99096
100 ppm	68.63	0.01068	0.9464	92.51	0.00022	0.99446

is close to the q_e value calculated by the quasi-second-order kinetic equation. This result shows that the quasi-second-order kinetic equation of Lagergren can well simulate the adsorption of Cu(II) ions by GA-CDA/HBP-NH$_2$, and the adsorption of Cu(II) ions by GA-CDA/HBP-NH$_2$ belongs to chemical adsorption.

The adsorption data of Cr(VI) ions with different concentrations of adsorbents are fitted, and the relevant data are shown in Table 3. As shown in Table 3, R^2 obtained by the quasi-second-order kinetic equation regression fitting is greater than 0.990, which is better than that obtained by quasi-first-order kinetic equation, and the equilibrium adsorption capacity of Cr(VI) ions obtained from heavy metal adsorption experiments is close to the q_e value calculated by the quasi-second-order kinetic equation. The quasi-second-order kinetic equation of Lagergren can well simulate the adsorption of Cr(VI) ions by GA-CDA/HBP-NH$_2$, and the adsorption of Cr(VI) ions by GA-CDA/HBP-NH$_2$ belongs to chemical adsorption.

Fig. 11 SEM images of CDA and GA-CDA/HBP-NH$_2$ after adsorption of heavy metals: (a and b) adsorption of Cu(II), (c and d) adsorption of Cr(VI), (a and c) CDA, and (b and d) GA-CDA/HBP-NH$_2$ nanofibers.

3.3. SEM image and EDS mapping of CDA and GA-CDA/HBP-NH$_2$ after adsorption of heavy metals

The surface morphology of CDA and GA-CDA/HBP-NH$_2$ was imaged by SEM and EDS to confirm the adsorption of Cu(II) and Cr(VI) ions. Fig. 11 shows the SEM diagram of the nanofiber membrane after adsorption of heavy metals. As shown in Fig. 11(a and c), the surface of the CDA fiber is relatively smooth, without metal aggregates of Cu(II) and Cr(VI) ions, indicating that the adsorption effect of CDA is poor. Fig. 9(b and d) shows a large number of metal aggregates on the fiber surface because of the presence of HBP-NH$_2$ on the fiber membrane surface; therefore, the fiber membrane has adsorption properties.

Fig. 12(a and b) shows the EDS diagram of Cu(II) ion adsorption. Cu is evenly distributed on the surface of the adsorbed GA-CDA/HBP-NH$_2$, indicating that the modified adsorbent has an effect on Cu(II). Ion has a good adsorption effect. Fig. 12(c and d) shows the EDS diagram of adsorbing
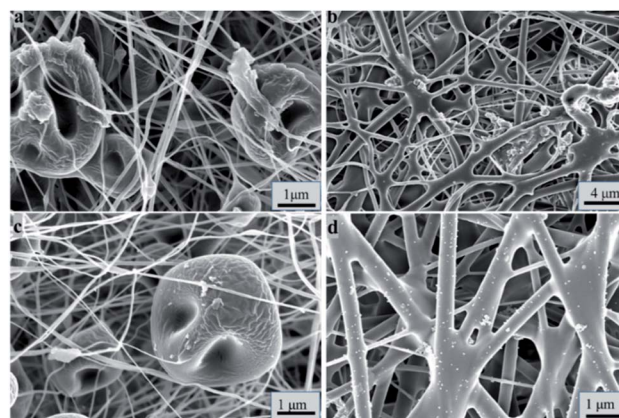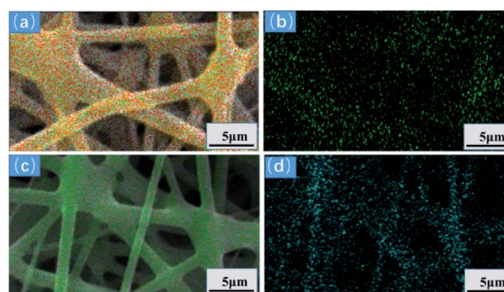

Fig. 12 EDS mapping of nanofibers adsorbing heavy metal ions: (a) Cu(II), (b) Cu(II) distribution, (c) Cr(VI), and (d) Cr(VI) distribution.

Cr(VI) ions. The surface of the adsorbed GA-CDA/HBP-NH$_2$ is evenly distributed with Cr. The latter adsorbent has a good adsorption effect on Cr(VI) ions.

4. Conclusion

Amino-rich GA-CDA/HBP-NH$_2$ nanofiber membranes were successfully prepared to remove heavy metal ions from water. The GA-CDA/HBP-NH$_2$ nanofiber membrane was characterized by SEM, FT-IR, XPS, EDS, and other testing methods, and these methods confirmed that GA was successfully crosslinked CDA/HBP-NH$_2$. The adsorption behavior of metal ions on the GA-CDA/HBP-NH$_2$ adsorbent was studied by constant temperature oscillation adsorption. The results of adsorption experiments showed that the optimum pH for adsorption of Cu(II) and Cr(VI) was 5.5 and 4.0, and the best adsorption time for Cu(II) and Cr(VI) was 480 and 240 min, respectively. When the amount of adsorbent was 0.01 g, the optimum concentration of Cu(II) and Cr(VI) ions in the initial solution was 80 mg L^{-1}. The adsorption performance of the GA-CDA/HBP-NH$_2$ membrane for Cr(VI) was better than that for Cu(II). The adsorption kinetics analysis showed that the adsorption isotherms of Cu(II) and Cr(VI) ions were in accordance with the Freundlich model, and the adsorption process was in accordance with the Lagergren quasi-second-order kinetic model. Therefore, the GA-CDA/HBP-NH$_2$ nanofiber membrane had great application potential.

Conflicts of interest

There are no conflicts to declare.

Acknowledgements

Notes and references

1 X. Huang, M. Sillanpaa, B. Duo and E. T. Gjessing, *Environ. Pollut.*, 2008, **156**, 270–277.
2 S. Rezania, S. M. Taib, M. F. M. Din, F. A. Dahalan and H. Kamyab, *J. Hazard. Mater.*, 2016, **318**, 587–599.
3 P. R. Gogate and A. B. Pandit, *Adv. Environ. Res.*, 2004, **8**, 553–597.
4 U. S. Toti and T. M. Aminabhavi, *J. Membr. Sci.*, 2004, **228**, 199–208.
5 M. Al-Shannag, Z. Al-Qodah, K. Bani-Melhem, M. R. Qtaishat and M. Alkasrawi, *Chem. Eng. J.*, 2015, **260**, 749–756.
6 N. Ghaemi, S. S. Madaeni, P. Daraei, H. Rajabi, S. Zinadini, A. Alizadeh, R. Heydari, M. Beygzadeh and S. Ghouzivand, *Chem. Eng. J.*, 2015, **263**, 101–112.
7 E. Igberase, P. Osifo and A. Ofomaja, *J. Environ. Chem. Eng.*, 2014, **2**, 362–369.
8 E. Haque, V. Lo, A. I. Minett, A. T. Harris and T. L. Church, *J. Mater. Chem. A*, 2014, **2**, 193–203.
9 G. Crini, *Prog. Polym. Sci.*, 2005, **30**, 38–70.
10 N. Wu, H. Wei and L. Zhang, *Environ. Sci. Technol.*, 2012, **46**, 419–425.
11 A. Alsbaiee, B. J. Smith, L. Xiao, Y. Ling, D. E. Helbling and W. R. Dichtel, *Nature*, 2016, **529**, 190-U146.
12 D. Qin, W. Lu, X. Wang, N. Li, X. Chen, Z. Zhu and W. Chen, *ACS Appl. Mater. Interfaces*, 2016, **8**, 25962–25970.
13 S. Peng, G. Jin, L. Li, K. Li, M. Srinivasan, S. Ramakrishna and J. Chen, *Chem. Soc. Rev.*, 2016, **45**, 1225–1241.
14 X. Lu, C. Wang and Y. Wei, *Small*, 2009, **5**, 2349–2370.
15 X. Lu, C. Wang, F. Favier and N. Pinna, *Adv. Energy Mater.*, 2017, **7**, 1601301.
16 D. Li and Y. Xia, *Nano Lett.*, 2003, **3**, 555–560.
17 O. K. Pereao, C. Bode-Aluko, G. Ndayambaje, O. Fatoba and L. F. Petrik, *J. Polym. Environ.*, 2017, **25**, 1175–1189.
18 S. S. Ray, S.-S. Chen, C.-W. Li, N. Nguyen Cong and N. Hau Thi, *RSC Adv.*, 2016, **6**, 85495–85514.
19 Y. Huang, Y.-E. Miao and T. Liu, *J. Appl. Polym. Sci.*, 2014, **131**, 40864.
20 F. E. Ahmed, B. S. Lalia and R. Hashaikeh, *Desalination*, 2015, **356**, 15–30.
21 X. Chen, G. Chen and P. L. Yue, *Environ. Sci. Technol.*, 2002, **36**, 778–783.
22 Y. Chen, L. Wang, H. Yu, Y. Zhao, R. Sun, G. Jing, J. Huang, H. Khalid, N. M. Abbasi and M. Akram, *Prog. Polym. Sci.*, 2015, **45**, 23–43.
23 Y. Zheng, S. Li, Z. Weng and C. Gao, *Chem. Soc. Rev.*, 2015, **44**, 4091–4130.
24 M. B. Camarada, M. Zuniga, J. Alzate-Morales and L. S. Santos, *Chem. Phys. Lett.*, 2014, **616**, 171–177.
25 Z. Zarghami, A. Akbari, A. M. Latifi and M. A. Amani, *Bioresour. Technol.*, 2016, **205**, 230–238.
26 C. Zang, Y. Ren, F. Wang, H. Lin and Y. Chen, *J. Eng. Fibers Fabr.*, 2016, **11**, 9–18.
27 H. Tian, L. Yuan, J. Wang, H. Wu, H. Wang, A. Xiang, B. Ashok and A. V. Rajulu, *J. Hazard. Mater.*, 2019, **378**, 120751.
28 D. Zhang, L. Chen, C. Zang, Y. Chen and H. Lin, *Carbohydr. Polym.*, 2013, **92**, 2088–2094.
29 L. Lv, J. Zhang, S. Yuan, L. Huang, S. Tang, B. Liang and S. O. Pehkonen, *RSC Adv.*, 2016, **6**, 78136–78150.